Charge Density of L-Alanyl-glycyl-L-alanine Based on X-Ray Data Collection Periods from 4 to 130 Hours

Diana Förster[a], Armin Wagner[b], Christian B. Hübschle[a], Carsten Paulmann[c], and Peter Luger[a]

[a] Institut für Chemie und Biochemie/Kristallographie, Freie Universität Berlin, Fabeckstraße 36a, D-14195 Berlin, Germany
[b] Swiss Light Source (SLS) at the Paul-Scherrer Institute, Villigen, Switzerland, and Diamond Light Source, Harwell Science and Innovation Campus, Diamond House, Chilton, Didcot, Oxfordshire, OX11 0DE, Great Britain
[c] Mineralogisch-Petrologisches Institut, Universität Hamburg, Grindelallee 48, D-20146 Hamburg, Germany

Reprint requests to Prof. Dr. Peter Luger. Fax: +49-30-838 53464. E-mail: luger@chemie.fu-berlin.de

Z. Naturforsch. **2007**, *62b,* 696 – 704; received November 21, 2006

The charge density of the tripeptide L-alanyl-glycyl-L-alanine was determined from three X-ray data sets measured at different experimental setups and under different conditions. Two of the data sets were measured with synchrotron radiation (beamline F1 of Hasylab/DESY, Germany and beamline X10SA of SLS, Paul-Scherer-Institute, Switzerland) at temperatures around 100 K while a third data set was measured under home laboratory conditions (MoK_α radiation) at a low temperature of 20 K. The multipole refinement strategy to derive the experimental charge density was the same in all cases, so that the obtained charge density properties could directly be compared. While the general analysis of the three data sets suggested a small preference for one of the synchrotron data sets (Hasylab F1), a comparison of topological and atomic properties gave in no case an indication for a preference of any of the three data sets. It follows that even the 4 h data set measured at the SLS performed equally well compared to the data sets of substantially longer exposure time.

Key words: Tripeptides, Charge Density, Topological Analysis, Synchrotron Radiation

Introduction

Already in 1915, hence three years after the discovery of X-ray diffraction, Peter Debye made a note [1] that the distribution of charge density should be obtainable from this new experimental method. However, it was a long way from Debye's vision in 1915 until the present stage of charge density work. Thanks to the technical developments in the last decade the exposure time of high resolution X-ray diffraction experiments has been reduced significantly so that experimental charge density determination on larger molecules or on series of chemically related compounds can be carried out in a reasonable time.

The introduction of Bader's quantum theory of atoms in molecules (QTAIM) [2] enables the quantitative derivation of bonding, non bonding and atomic properties from the topological analysis of a charge density distribution $\rho(\boldsymbol{r})$. A key concept in Bader's theory is the transferability and additivity of topological properties of submolecular fragments. Based on this concept various data base approaches have been developed [3 – 5] for a modelling of the charge densities of larger macromolecules, like proteins or other oligomers, which are otherwise obtainable only in exceptional cases [6, 7].

Regarding these developments the experimental verification of the transferability concept is of major importance. This can be performed by series of charge density studies in a given class of chemical compounds as has been done for the experimentally derived topological properties of 16 of the 20 genetically encoded amino acids [8].

The measure of transferability has also to be seen with respect to the reproducibility of topological data. We have addressed this question in a further comparative charge density study in the oligopeptide field, in that tripeptides of the type L-Ala-*Xxx*-L-Ala were considered, where *Xxx* was to be varied among the 20 naturally occurring amino acids. Two studies of that type have been published recently, one with *Xxx* = L-Ala [9]

and the second one on two modifications with *Xxx* = L-Tyr [10].

Here we present as a third example the results for L-alanyl-glycyl-L-alanine, where a major question was, how fast a charge density data collection can be to lead to an acceptable accuracy. This was studied for three data sets of the title tripeptide measured under different experimental conditions and at exposure times from 4 to 130 h.

Two of the data sets were measured with synchrotron radiation at the Hasylab/DESY (Hamburg, Germany, hereafter called Hasylab data set) and the Swiss Light Source (SLS; Paul-Scherrer-Institute, Villingen, Switzerland, SLS data set), while the third one was measured with MoK_α radiation under home laboratory conditions, where we are able to collect 20 K data sets (home data set). The two synchrotron setups were equipped with nitrogen gas stream cooling devices for measurements around 100 K.

Results and Discussion

Data set considerations

In order to examine the quality of the three data sets we discuss the commonly used figures of merit (based on multipole refinements with exactly the same models in all three cases, see Experimental Section) compared to the amount of collected reflections and derived properties like completeness or redundancy.

As summarized in Table 1, the three data sets are very different. The total number of reflections varies from 28000 (SLS) to almost the fourfold number for the Hasylab data. Nevertheless the latter one shows the best agreement factors and also redundancy (close to 10), completeness and the reflection to parameter ratio (N_{ref}/N_{var} = 21) are the highest among the three data sets.

With respect to the amount of data the SLS figures of merit have to be considered with care. The reduced resolution and the relatively small number of reflections cause smaller completeness, redundancy and N_{ref}/N_{var}. Since low resolution data tend to lower R values, the comparably small R value after multipole refinement has to be seen in relation to the limited data.

As already mentioned above, the multipole refinements were carried out with exactly the same model for all three data sets, that means with the same assignment of constraints and local symmetry. It was also attempted to refine all data sets without any constraints and symmetry assumptions. The refinement was stable for the Hasylab and home data but did not converge satisfactorily for the SLS data set. While the limitations of the SLS data set can on the one hand not be overlooked, it has on the other hand to be noted that the whole measurement at the SLS took only 4 h. Moreover, as will be shown below, the derived quantitative tolopogical properties are not inferior compared, for example, to the Hasylab measurement. With respect to amount of data and figures of merit the conventional home data set performs between both synchrotron data sets.

As a further criterion for the accuracy of the different experiments and the reliability of the multipole model the residual density, being the Fourier transform of the $F_o - F_c$ differences, can be utilized. A three-dimensional distribution of residual density was calculated at different resolutions, and the main results are shown in Table 2.

For the full order data, which are not available in the SLS case, the residual density is satisfactorily low for the Hasylab data. If the resolution cut off is lowered,

Table 1. Amount of data and figures of merit of the three data sets of Ala-Gly-Ala.

	Home	Hasylab	SLS
Exposure time [h]	130	28	4
Max $\sin\theta/\lambda$ [Å^{-1}]	1.18	1.25	0.98
Total no. of reflections	32605	97469	28133
No. of unique reflections	7601	9450	4467
R_{int}	0.028	0.042	0.032
Completeness [%]	89.9	97.8	77.3
Redundancy	4.4	10.3	6.3
R_1/R_{all} [%]	3.6/4.75	2.6/3.94	2.7/3.09
R_w [%]	2.33	2.15	3.89
N_{ref}/N_{var} [a]	17	21	12
GoF	1.9	2.1	2.9

[a] N_{ref}/N_{var} is the ratio of reflections to parameters.

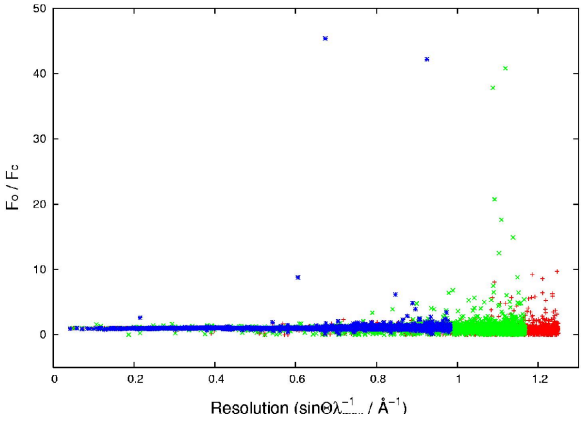

Fig. 1. Ratio F_o/F_c plotted *vs.* resolution for the three data sets. Color code: Hasylab = red, Home = green, SLS = blue.

Table 2. *R* values and residual densities (RD) with different cut off. RMS: root mean square density.

	Home	Hasylab	SLS	Home	Hasylab	SLS	Home	Hasylab	SLS
	– data up to 1.2 Å^{-1} –			– data up to 1.0 Å^{-1} –			– data up to 0.9 Å^{-1} –		
R_1 %	3.6	2.5	–	2.2	1.7	2.7	1.8	1.4	2.6
RD max [e Å^{-3}]	0.56	0.20	–	0.23	0.14	0.28	0.18	0.13	0.25
RD min [e Å^{-3}]	−0.32	−0.25	–	−0.21	−0.16	−0.24	−0.13	−0.15	−0.23
RMS [e Å^{-3}]	0.085	0.041	–	0.043	0.030	0.053	0.033	0.027	0.047

as is sometimes applied as a cosmetic trick to smooth the residual density, reliability factors and magnitudes of residual density decrease, while the performance of the Hasylab data is still the best.

An overall impression of the data set quality is given in the diagram of Fig. 1 which shows the ratios F_o/F_c *vs*. the resolution. Theoretically, a horizontal line around $F_o/F_c = 1$ results in case of perfect data. Experimentally, the more the resolution increases the more the quality decreases, thus the distribution at the end of the line widens. This spread can be taken as a measure of quality loss. A linear spread *vs.* resolution relationship without any outliers would indicate experimental data of high quality. As shown in the diagram, the quality of all three data sets is very good. However, it can be seen that the Hasylab data (in red), although having the highest resolution have the fewest overall outliers. Furthermore, the line spread in the high resolution region is the smallest of the three data sets. Less accuracy is shown in the plot of SLS data (blue squares). The diagram shows some outliers even in the low resolution region. The green crosses visualise the home data set. As discussed earlier, its quality seems to be between the two synchrotron data sets. Its spread is more pronounced than in the case of the Hasylab data, but the outliers do not start before $\sin\theta/\lambda = 1.1$ Å^{-1}.

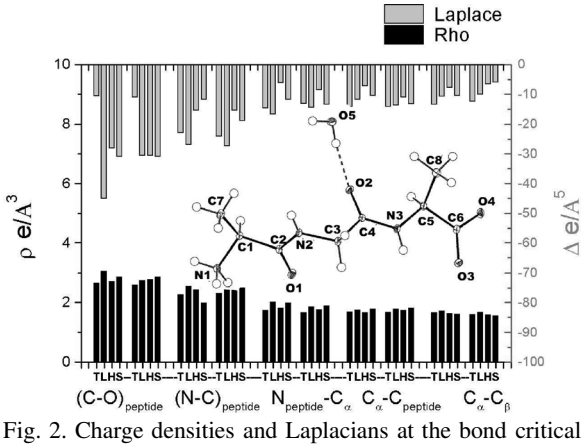

Fig. 2. Charge densities and Laplacians at the bond critical points in the tripeptide main chain. The three data sets and the theoretical results are represented in four columns for each bond: first column gives theory (T), the second column gives the Home laboratory (L) values, the third one shows the Hasylab (H) values and the last column the ones of the SLS (S) data set.

Bond topological analysis

The bond topological analysis of the experimental $\rho(\boldsymbol{r})$ was carried out with the XDPROP part of the XD [11] program system. All expected bond critical points (bcp's, defined by the property that the gradient $\nabla\rho(\boldsymbol{r})$ vanishes at a bcp) could be located. For comparison theoretical bcp's from a B3LYP calculation were also derived.

An estimate of the accuracy and the reproducibility obtainable from the three experiments can be derived from averaging over the electron density values ρ(bcp) and the Laplacians $\nabla^2\rho$(bcp) at the bond critical points of the 14 non H bonds. The corresponding data are listed in Table 3, which gives also the average of the three experimental contributions to each bond with the corresponding standard deviation σ_n $\left[\sigma_n = \{1/3\sum_{i=1}^{3}(x_i - \bar{x})^2\}^{1/2}\right]$ in parentheses. If we average over the 14 σ_n values we get mean values of 0.069 e Å^{-3} for the electron density and 3.4 e Å^{-5} for the Laplacians. These quantities are in the same range as reported in the literature for the reproducibility of these topological descriptors [10] and the uncertainty range is that given by several authors [12 – 14] to be considered if electron density results from different experiments are to be compared.

We have also calculated the average differences between experimental and theoretical ρ(bcp)'s and corresponding Laplacians ($\nabla^2\rho$(bcp)'s) for the fourteen bonds. For ρ(bcp) the average differences between experiment and theory are 0.25/0.14/0.22 e Å^{-3} for the home/Hasylab/SLS data, for the Laplacians we get 9.5/9.8/7.5 e Å^{-5}. The latter ones are unexpectedly high, which is mainly caused by rather high experimental/theoretical discrepancies in the six C–O bonds. If they are left out from the averaging the (exp–theo) differences for the Laplacians of the 10 non C–O bonds

Table 3. Topological properties.

First line ρ(bcp) in e Å^{-3}, second line $\nabla^2\rho$(bcp) in e Å^{-5}.

Bond type		Home	Hasylab	SLS	Average (σ_N)	Theory
$(C–O)_{pep}$	O1–C2	3.11(5)	3.02(3)	2.86(6)	3.00(10)	2.66
		−42.3(3)	*−35.6(2)*	*−27.9(4)*	*−35(6)*	*−10.7*
	O2–C4	3.07(5)	2.97(3)	2.81(6)	2.95(11)	2.59
		−41.2(3)	*−34.0(2)*	*−26.2(4)*	*−34(6)*	*−11.1*
$(C–N)_{pep}$	N2–C2	2.55(5)	2.43(2)	2.50(5)	2.50(5)	2.28
		−27.1(2)	*−15.5(2)*	*−19.0(2)*	*−21(5)*	*−23.0*
	N3–C4	2.57(5)	2.44(2)	2.52(5)	2.51(5)	2.32
		−27.6(2)	*−15.5(2)*	*−19.5(2)*	*−21(5)*	*−24.2*
$C_\alpha–N_{pep}$	N2–C3	2.02(4)	1.82(3)	1.99(6)	1.94(9)	1.74
		−16.8(2)	*−16.8(1)*	*−11.9(2)*	*−15(2)*	*−14.9*
	N3–C5	1.86(4)	1.78(3)	1.90(6)	1.85(5)	1.67
		−14.6(2)	*−8.7(2)*	*−13.6(2)*	*−12(3)*	*−13.3*
$C_\alpha–C_{pep}$	C1–C2	1.76(3)	1.67(2)	1.79(4)	1.74(5)	1.69
		−11.9(1)	*−7.4(1)*	*−10.6(1)*	*−10(2)*	*−14.4*
	C3–C4	1.79(4)	1.75(3)	1.81(5)	1.78(3)	1.68
		−13.9(1)	*−11.2(1)*	*−13.4(1)*	*−13(1)*	*−14.3*
$C_\alpha–C_\beta$	C1–C7	1.73(3)	1.64(2)	1.61(4)	1.66(5)	1.66
		−10.9(1)	*−7.9(1)*	*−7.2(1)*	*−9(2)*	*−13.6*
	C5–C8	1.69(3)	1.59(1)	1.57(4)	1.61(5)	1.60
		−10.1(1)	*−6.8(1)*	*−6.1(1)*	*−8(2)*	*−12.6*
$(C–O)_{carboxyl}$	C6–O3	3.06(6)	2.72(4)	2.87(8)	2.88(14)	2.48
		−45.2(4)	*−28.3(2)*	*−31.2(4)*	*−35(7)*	*−12.2*
	C6–O4	2.74(6)	2.78(4)	2.91(9)	2.81(7)	2.54
		−30.7(4)	*−30.8(2)*	*−34.1(4)*	*−32(2)*	*−11.8*
$C_\alpha–N_{ammonium}$	C1–N1	1.82(3)	1.70(2)	1.84(5)	1.78(6)	1.59
		−13.2(2)	*−7.6(1)*	*−13.0(2)*	*−11(3)*	*−12.2*
	C5–C6	1.85(3)	1.69(2)	1.83(5)	1.79(7)	1.68
		−12.7(1)	*−7.5(1)*	*−11.9(2)*	*−11(2)*	*−12.6*

Table 4. Averaged values of electron density and Laplacian at the BCPs for the different bond types in the three data sets (first line), with corresponding averages from the literature [10]; n = no. of contributing data.

Bond type	n	ρ(bcp) (e Å^{-3})	$\nabla^2\rho$(bcp) (e Å^{-5})
$(C–O)_{pep}$	6	2.79(10)	−35(6)
	8	2.90(7)	−31(6)
$(C–N)_{pep}$	6	2.50(5)	−21(5)
	8	2.44(4)	−23(3)
$C_\alpha–N_{pep}$	6	1.90(8)	−14(3)
	8	1.82(4)	−11(2)
$C_\alpha–C_{pep}$	6	1.76(5)	−11(2)
	8	1.71(5)	−11(2)
$C_\alpha–C_\beta$	6	1.64(6)	−8(2)
	12	1.64(6)	−10(2)

reduce to 2.0/5.4/3.1 e Å^{-5} for the home/Hasylab/SLS data. Nevertheless, no indication for a preference for any of the three data sets in seen.

Fig. 2 shows the values of the electron density at the bcp's and the corresponding Laplacians for the 10 bonds of the tripeptide main chain. In the tripeptide, there are two peptide bond regions, so that transferability between the same bond types of the same submolecular fragment (column blocks close to each other), can be examined. For the three experimental data sets the average difference between chemically equivalent bond pairs in the peptide bond regions is between 0.05 and 0.06 e Å^{-3} for ρ(bcp), and between 1.3 and 2.9 e Å^{-5} for $\nabla^2\rho$(bcp). Also no preference for one of the data sets can be found. Table 4 shows that for the bonds in the peptide bond region, if averaged over the three experiments (hence 6 data per entry), the bond topological properties compare very well with the corresponding averages recently reported for the Ala-*Xxx*-Ala class of compounds [10].

Atomic properties

Bader's AIM theory provides a well defined procedure of partitioning a molecule into atomic regions. According to Bader, an atom is the union of a nuclear critical point [(3; −3) critical point] and its associated basin of attracted trajectories of the electron density gradient vector field $\nabla\rho(\boldsymbol{r})$ with zero flux surfaces (ZFS) as boundaries. The integration procedure available through the TOPXD program was applied to eval-

Atom	V_{tot} Home	V_{tot} Hasylab	V_{tot} SLS	V_{001} Home	V_{001} Hasylab	V_{001} SLS	Q Home	Q Hasylab	Q SLS
O(1)	17.64	16.80	17.42	17.08	15.88	16.45	−1.18	−1.05	−1.16
O_{pep1}	17.3(4)			16.5(5)			−1.13(6)		
O(2)	17.86	17.24	17.85	15.01	14.43	15.07	−1.05	−0.96	−1.03
O_{pep2}	17.7(3)			14.8(3)			−1.01(4)		
O(3)	16.04	15.51	15.93	15.59	14.89	15.48	−1.19	−0.96	−1.02
$O_{carboxy}$	15.8(2)			15.3(3)			1.06(9)		
O(4)	20.20	18.79	19.87	17.00	16.08	17.13	−1.10	−0.98	−1.05
$O_{carboxy}$	19.6(6)			16.7(5)			1.04(5)		
O(5)	25.14	23.22	23.60	20.10	19.18	19.59	−1.69	−1.39	−1.37
$O_{solvent}$	24.0(8)			19.6(4)			−1.4(3)		
N(1)	17.11	14.82	14.60	16.33	14.08	13.94	−1.72	−1.28	−1.13
N_{ammoni}	16(1)			15(1)			1.4(3)		
N(2)	14.27	13.37	13.43	13.95	13.02	13.19	−1.28	−1.02	−1.12
N_{pep1}	13.7(4)			13.4(4)			−1.1(1)		
N(3)	15.15	14.77	14.74	14.19	13.02	13.73	−1.24	−1.00	−1.10
N_{pep2}	14.9(2)			13.7(5)			−1.1(1)		
C(1)	6.94	6.54	6.90	6.92	6.53	6.90	0.17	0.24	0.13
C_α	6.8(2)			6.8(2)			0.18(5)		
C(2)	4.93	5.95	5.80	4.93	5.94	5.80	1.34	0.93	1.00
C_{pep1}	5.6(5)			5.6(5)			1.1(2)		
C(3)	8.83	8.51	9.22	8.54	8.20	8.84	0.12	0.19	0.11
$C_{\alpha+1}$	8.9(3)			8.5(3)			0.14(4)		
C(4)	7.40	7.47	7.39	6.48	6.43	6.46	0.89	0.89	0.95
C_{pep2}	7.4(4)			6.5(2)			0.91(3)		
C(5)	7.19	6.80	7.14	7.03	6.66	7.03	0.19	0.24	0.12
$C_{\alpha+2}$	7.0(2)			6.9(2)			0.18(5)		
C(6)	6.14	6.22	5.52	5.87	5.91	5.36	1.20	1.18	1.39
$C_{carboxy}$	6.0(3)			5.7(3)			1.26(9)		
C(7)	10.20	10.96	10.99	9.55	9.74	9.78	0.09	0.11	0.24
C_β	10.7(4)			9.7(1)			0.15(7)		
C(8)	11.73	11.59	12.00	9.51	9.75	9.93	0.10	0.14	0.23
$C_{\beta+2}$	11.8(2)			9.7(2)			0.16(5)		
Sum[a]	284.52	284.18	283.32				0.02	0.04	0.08

Table 5. First line: Atomic properties of the two peptide groups derived from QTAM for Home, Hasylab and SLS data sets. Second line: Atom type and averages of the three contributions. (Units are given in Å^3 and e).

[a] All atoms included.

uate atomic volumes and charges. The results are summarized for all three data sets of the title compound in Table 5. While the total atomic volumes V_{tot} are defined by the interatomic boundaries in the crystal, it is common practise to consider also the V_{001} volumes, defined by a cut off at $\rho = 0.001$ au, which are useful for comparison with corresponding properties of isolated molecules. Since the charge density in the outer regions of an atomic basin does not contribute substantially to its charge, Q_{tot} and Q_{001} values are practically equal so that only one charge column is given in Table 5.

Bader volumes and charges are additive so that the charges should sum up to zero, and the sum of the V_{tot}'s (multiplied by $Z = 2$) should reproduce the unit cell volume. As shown by the last line in Table 5, this is satisfied for all three data sets of Ala-Gly-Ala (within 0.5 – 0.9 % for the volume and 0.02 – 0.08 e for the charge) indicating that the partitioning and integration procedure has worked properly.

If averagings and consideration of standard uncertainties are performed similarly as for the bonding properties to compare also atomic properties of the three data sets we obtain average e.s.d.'s of the three data sets of 0.4 Å^3 for V_{tot}, 0.4 Å^3 for V_{001} and 0.1 e for Q. Again these quantities are in line with the reproducibility we found in our earlier study on two modifications of Ala-Tyr-Ala and with several literature studies, where quantitative data of this type were compared [10].

For a further examination of transferability in the peptide main chain we have averaged over the atomic properties of the chemically equivalent atoms and compared the results with the corresponding findings for Ala-Tyr-Ala (Table 6). The agreement is in the expected range, within roughly 0.1 e and 1 Å for charges and volumes, respectively. An exception is the volume of the atom C_α of the glycyl residue which is larger than the corresponding Ala C_α atom by about 1.5 Å^3. This makes sense because the atom carries two hydro-

Table 6. Charges Q_{001} (e) and volumes V_{001} (Å^3) for the atoms in the peptide groups averaged over the three data sets of the title compound (first line) and corresponding averages from the literature [10] (second line), n = number of contributing data.

Atom	n	Q_{001}	V_{001}
C_α	6	0.18(5)	6.9(2)
	12	0.18(7)	7.0(3)
C_{pep}	6	1.00(16)	6.0(6)
	8	1.02(10)	6.3(4)
O_{pep}	6	−1.07(8)	15.7(9)
	8	−1.07(7)	15.7(6)
N_{pep}	6	−1.13(10)	13.5(5)
	8	−1.01(6)	12.6(2)

gen atoms which is not the case for all other amino acid residues.

It follows, that in total the variation of the central amino acid in the system Ala-*Xxx*-Ala has no influence, neither on bond nor atomic properties, within the accuracy of experimental electron density work reachable at present.

Electrostatic potential

The electrostatic potential (EP) was calculated from the experimental charge density using the method of Su and Coppens [15]. The results are displayed for all three data sets in Fig. 3 by a color code (see color bars) on the iso electron density surface at ρ = 0.5 e Å^{-3}. The color range was scaled to be the same in the three representations in order to allow a convenient comparison.

Within the graphical error the EP distributions on the three molecular surfaces are alike confirming the equivalence of the electronic properties of the tripeptide obtained from the three data sets. The EP makes the polarization of the electron density in certain regions of the molecule visible, in that, for example, positive charge is concentrated at the C-terminus while the carboxylate group and the peptide group oxygen atoms are the negatively charged regions.

Pronounced positive EP is found at the hydrogen atoms which are involved in intermolecular hydrogen bonding as is seen, for example, in the EP region between the solvent water molecule and the accepting oxygen atom of one peptide carbonyl group.

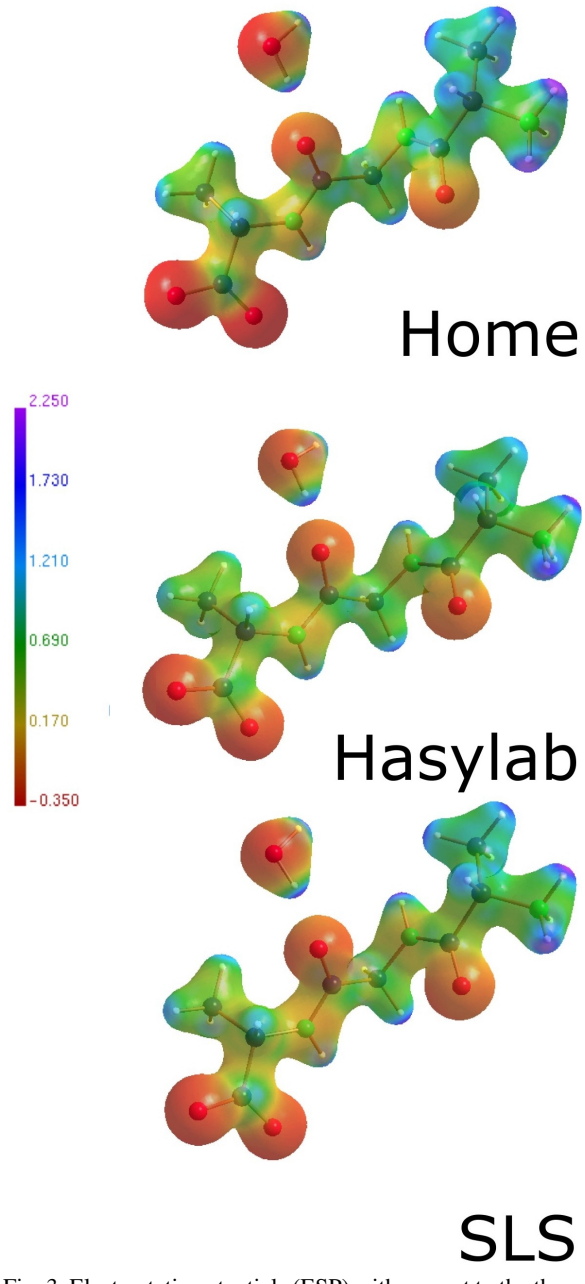

Fig. 3. Electrostatic potentials (ESP) with respect to the three data sets. The colour gradient ranges from −0.35 e Å^{-1} (red) up to 2.25 e Å^{-1} (purple). The three representations refer to Home lab data (top), Hasylab (middle) and SLS data (bottom). Representations generated with Mol*Iso* [16].

Conclusion

Three data sets of Ala-Gly-Ala were measured under very different experimental conditions with respect to diffractometer setup, radiation type and wavelength, detector type, temperature and beam time period, which varied between 4 h and more than 5 d. For the fastest data collection carried out at the SLS beamline X10SA the amount of data and the resolution

were the lowest. While this could have been expected to negatively influence the result, this expectation was not directly confirmed. A general analysis of the data sets (see, for example, Fig. 1) and inspection of the residual density results suggested on one hand that the SLS data behaved inferior to the home and Hasylab data. On the other hand, quantitative bond topological and atomic properties gave in no case an indication for a preference of any of the three data sets. All quantitative results were reproducible within the standard uncertainties.

Transferability of atomic and bonding properties in the peptide bond region was confirmed and the obtained quantities did not show significant differences to those which were recently derived on related tripeptides of the Ala-*Xxx*-Ala type with *Xxx* = Ala [9] and *Xxx* = Tyr [10]. Regarding the 130 h beam time period for the home lab data collection compared to the 4 h time frame at the SLS it seems – theoretically – possible to collect more than 30 charge density data sets at the latter in the time one home experiment takes without significant loss in quality.

Moreover, it should be stated that the above mentioned limitations of the SLS data collection are related to the typical experimental setting for a protein crystallography beamline which are mostly of mechanical nature and could be overcome with little effort to make also high-order regions of reciprocal space accessible. It follows that the execution of series of charge density studies of chemically or biologically related compounds is in sight, so that such studies in the electron density field can be expected in time periods presently needed for conventional spherical X-ray analyses.

Experimental Section

X-Ray experiments and multipole refinements

Crystals were grown by evaporation of a H_2O/DMF (20 : 1) solution of a commercially available sample of Ala-Gly-Ala (Bachem, Germany).

The home data set was collected at 20 K in our home laboratory with conventional MoK_α radiation on a Huber four circle diffractometer equipped with a closed cycle He cryostat, where a 0.1 mm Kapton film vacuum chamber around the cold head was used [17]. Frames were measured with a Bruker APEX CCD detector in φ scan modus with frame-to-frame increments of 0.3°.

The Hasylab data set was measured with synchrotron radiation (beamline F1 at Hasylab/DESY, Hamburg, Germany) at 100 K with nitrogen gas stream cooling, while the SLS data set was measured at beamline X10SA of the Swiss Light Source (SLS at the Paul-Scherrer-Institute, Villigen, Switzerland) [18]. For both synchrotron data collections MAR CCD detectors were used, type 165 at F1 und type 225 at X10SA. The MAR control and data processing software [19] allowed frame-to-frame increments of 3° enabling very short beamtime periods, so that combined with the high synchrotron primary intensities the exposure times were reduced to 28 h at F1 and even to 4 h at X10SA. Since station X10SA is a protein dedicated beam line the highest regions of reciprocal space could not be reached owing to geometrical restrictions so that compared to the two other data sets a few limitations in resolution ($\sin\theta/\lambda_{max} = 0.98$ Å^{-1}), completeness and redundancy had to be accepted.

Table 7. Measuring conditions of the three data sets of Ala-Gly-Ala.

	Home	Hasylab	SLS
Beamline	Huber (home)	F1	X10SA
Detector	APEX	MARCCD-165	MAR-CCD-225
Cooling system	He-cryostat	N_2-flow	N_2-flow
Temperature, K	20	100	92
Radiation type	MoK_α	synchrotron	synchrotron
Wavelength, Å	0.7107	0.55	0.6214
Frame-to-frame scan modus	φ	ω/φ	φ
Frame increments, deg	0.3	3	3

The SAINT and SADABS [20] software was applied for integration of the APEX data, while this was done with the XDS software for the integration of the MAR detector data. For a summary of experimental setups, see Table 7.

The results of a spherical structure determination have been reported elsewhere and need no further discussion here [21]. The Hansen-Coppens multipole formalism [22] as implemented in the XD program system [11] was then applied for aspherical refinement of all data sets with the spherical model used in the initial stage of refinement. The atomic electron density $\rho_a(\boldsymbol{r})$ in this model is

$$\rho_a(r) = \rho_{core}(r) + P_v \kappa^3 \rho_{val}(\kappa r) + \sum_{l=0}^{l\,\max} \kappa'^3 R_l(\kappa' r) \sum_{m=-1}^{1} P_{lm} Y_{lm}(\theta,\phi), \quad (1)$$

were the first two terms represent the spherical core and valence density and the last term accounts for aspherical contributions. In all cases the full matrix least squares program (XDLSM) of the XD package was used with statistical weights $w_H = \sigma^2\,(F_{obs}(H))$.

The chosen refinement procedure and the multipole model were exactly the same for all three data sets. Carbon, nitrogen and oxygen atoms were refined up to the hexadecapole level, while for hydrogen atoms additionally to monopole refinement only a bond directed dipole was refined. Hydrogen bond distances were fixed at neutron distances according to

their bond type as listed in the International Tables for X-ray crystallography [23].

According to the different hybridizations and atom types altogether 8 contraction/expansion parameters (κ) were introduced. For hydrogen atoms a fixed κ of 1.2 was used, while all other κ parameters were refined. For κ' energy optimized values were used. The resulting agreement factors for the three data sets are summarized in Table 1.

Theoretical calculations

Theoretical calculations were performed at the B3LYP density functional using the GAUSSIAN98 program [24]. A single point calculation was performed with the 6-311++G(3*df*,3*pd*) basis set at experimental geometry and allows a direct comparison of bond topological parameters with the experimental ones. Topological analysis was performed with MORPHY98 [25].

CCDC 278555, CCDC 627276 and CCDC 627277 contain the supplementary crystallographic data for this paper. These data can be obtained free of charge from The Cambridge Crystallographic Data Centre *via* www.ccdc.cam.ac.uk/data_request/cif.

Acknowledgement

The authors are grateful to the Deutsche Forschungsgemeinschaft (DFG) for financial support within the Lu 222/27-1 and SPP 1178 projects.

[1] P. Debye, *Annalen der Physik* **1915**, *46*, 809 – 823.
[2] R. F. W. Bader, *Atoms in Molecules – A Quantum Theory*, Clarendon Press, Oxford, **1990**, p. 1994.
[3] B. Dittrich, Ch. B. Hübschle, M. Messerschmidt, R. Kalinowski, D. Girnt, P. Luger, *Acta Crystallogr.* **2005**, *A61*, 314 – 320.
[4] A. Volkov, X. Li, T. Koritsánszky, P. Coppens, *J. Phys. Chem.* **2004**, *A108*, 4283 – 4300.
[5] V. Pichon-Pesme, C. Jelsch, B. Guillot, C. Lecomte, *Acta Crystallogr.* **2004**, *A60*, 204 – 208.
[6] D. Housset, F. Benabicha, V. Pichon-Pesme, C. Jelsch, A. Maierhofer, S. David, J. C. Fontecilla-Camps, *Acta Crystallogr.* **2000**, *D56*, 151 – 160.
[7] C. Jelsch, M. M. Teeter, V. Lamzin, V. Pichon-Pesme, R. H. Blessing, C. Lecomte, *Proc. Natl. Acad. Sci.* **2000**, *97*, 3171 – 3176.
[8] S. Mebs, M. Messerschmidt, P. Luger, *Z. Kristallogr.* **2006**, 656 – 664.
[9] E. Rödel, M. Messerschmidt, B. Dittrich, P. Luger, *Org. Biom. Chem.* **2006**, *4*, 475 – 481.
[10] L. Chęcińska, S. Mebs, Ch. B. Hübschle, D. Förster, W. Morgenroth, P. Luger, *Org. Biomol. Chem.* **2006**, *4*, 3242 – 3251.
[11] T. Koritsánszky, P. R. Mallison, S. T. Howard, A. Volkov, P. Macchi, Z. Su, C. Gatti, T. Richter, L. J. Farrugia, N. K. Hansen, X. D-A, Computer Program Package for Multipole Refinement and Analysis of Electron Densities from Diffraction Data, Freie Universität Berlin, Berlin (Germany) **2003**.
[12] V. Picon-Pesme, H. Lachekar, M. Souhasson, C. Lecomte, *Acta Crystallogr.* **2000**, *B56*, 728 – 737.
[13] B. Dittrich, T. Koritsánszky, M. Grosche, W. Scherer, R. Flaig, A. Wagner, H. G. Krane, H. Kessler, C. Riemer, A. M. M. Schreurs, P. Luger, *Acta Crystallogr.* **2002**, *B58*, 721 – 727.
[14] M. Messerschmidt, S. Scheins, P. Luger, *Acta Crystallogr.* **2005**, *B61*, 115 – 121.
[15] Z. Su, P. Coppens, *Acta Crystallogr.* **1992**, *A48*, 188 – 197.
[16] Ch. B. Hübschle, P. Luger, *J. Appl. Crystallogr.* **2006**, *39*, 901 – 904.
[17] M. Messerschmidt, M. Meyer, P. Luger, *J. Appl. Crystallogr.* **2003**, *36*, 1452 – 1454.
[18] E. Pohl, C. Pradervand, R. Schneider, T. Tomizaki, A. Paulhuhn, Q. Chen, G. Ingold, E. Zimoch, C. Schulze-Briese, *Synchrotron Radiation News* **2006**, *19*, 24 – 26.
[19] W. Kabsch, *J. Appl. Crystallogr.* **1993**, *26*, 795 – 800.
[20] ASTRO (**1995** – **1996**), SMART (**1996**), SAINT (**1994** – **1996**), Bruker AXS Inc., Madison, Wisconsin (USA).
[21] D. Förster, M. Messerschmidt, P. Luger, *Acta Crystallogr.* **2005**, *C61*, 420 – 421.
[22] N. K. Hansen, P. Coppens, *Acta Crystallogr.* **1978**, *A34*, 909 – 921.
[23] A. J. C. Wilson, *International Tables for X-Ray Crystallography*, Vol. C, *Mathematical, Physical and Chemical Tables*, Kluwer Academic Publishers, Dordrecht, **1992**.
[24] M. J. Frisch, G. W. Trucks, H. B. Schlegel, G. E. Scuseria, M. A. Robb, J. R. Cheeseman, V. G. Zakrzewski, J. A. Montgomery (Jr.), R. E. Stratmann, J. C. Burant, S. Dapprich, J. M. Millam, A. D. Daniels, K. N. Kudin, M. C. Strain, O. Farkas, J. Tomasi, V. Barone, M. Cossi, R. Cammi, B. Mennucci, C. Pomelli, C. Adamo, S. Clifford, J. Ochterski, G. A. Petersson, P. Y. Ayala, Q. Cui, K. Morokuma, D. K. Malick, A. D. Rabuck, K. Raghavachari, J. B. Foresman, J. Cioslowski, J. V. Ortiz, A. G. Baboul, B. B. Stefanov, G. Liu, A. Liashenko, P. Piskorz, I. Komaromi, R. Gomperts, R. L. Martin, D. J. Fox, T. Keith, M. A.

Al-Laham, C. Y. Peng, A. Nanayakkara, C. Gonzalez, M. Challacombe, P. M. W. Gill, B. Johnson, W. Chen, M. W. Wong, J. L. Andres, M. Head-Gordon, E. S. Replogle, J. A. Pople, Gaussian 98, (Revision A.7), Gaussian Inc., Pittsburgh, Pennsylvania (USA) **1998**.

[25] MORPHY98, A program written by P. L. A. Popelier with a contribution from R. G. A. Bone, UMIST, Manchester, England (U. K.) **1998**.